

## Thiophene-Based Covalent Organic Frameworks

Guillaume V. H. Bertrand, Vladimir K. Michaelis, Ta-Chung Ong, Robert G. Griffin, and Mircea Dincă\*

*Department of Chemistry and Francis Bitter Magnet Laboratory  
Massachusetts Institute of Technology  
Cambridge, MA 02139, United States of America*

### *Supporting Information*

[mdinca@mit.edu](mailto:mdinca@mit.edu)

#### **Index**

<b>A. Materials and measurements</b> .....	1
<b>B. Methodology for T-COF Synthesis.</b> .....	4
<b>C. Figures</b> .....	6

#### **A. Materials and measurements**

Starting materials were purchased from Sigma-Aldrich or TCI and used without further purification. Mesitylene and 1,4-dioxane were purchased from TCI. *N,N*-dimethylformamide, hexane, ethyl acetate and silica-gel were purchased from VWR. THF was taken from an alumina column solvent purification system. NMR spectra were recorded on a Varian 300 Mercury NMR spectrometer and a Bruker Avance-400 NMR spectrometer. <sup>1</sup>H NMR data are reported as follows: chemical shift (multiplicity (s = singlet, d = doublet, b = broad), integration, coupling constants). <sup>1</sup>H and <sup>13</sup>C chemical shifts are reported in ppm from TMS with the residual solvent resonances as internal standards. Elemental analyses were performed by Midwest Microlab.

Thermogravimetric analysis (TGA) was performed on a TA Instruments Q500 Thermogravimetric Analyzer at a heating rate of 0.5°C/min under a nitrogen gas flow of 90 mL/min on a platinum pan. Powder X-ray diffraction (PXRD) patterns were recorded with a Bruker D8 Advance diffractometer equipped with a  $\theta/2\theta$  Bragg-Brentano geometry and nickel-filtered Cu K $\alpha$  radiation ( $K\alpha_1 = 1.5406 \text{ \AA}$ ,  $K\alpha_2 = 1.5444 \text{ \AA}$ ,  $K\alpha_1/K\alpha_2 = 0.5$ ). The tube voltage and current were 40 kV and 40 mA, respectively.

Samples for PXRD were prepared by placing a thin layer of the designated materials on a zero-background silicon (510) crystal plate.

A Micromeritics ASAP 2020 Surface Area and Porosity Analyzer was used to measure the nitrogen adsorption isotherm. An oven-dried sample tube equipped with a TranSeal™ (Micromeritics) was evacuated and tared. The sample was transferred to the sample tube, which was then capped by a TranSeal™. The sample was heated to 200°C under a vacuum of 2 mtorr for 12 hours, at which point the outgas rate was less than 2 mtorr/minute. The evacuated sample tube was weighed again and the sample mass was determined by subtracting the mass of the previously tared tube. The N<sub>2</sub> isotherm was measured using a liquid nitrogen bath (77 K). Ultra high purity grade (99.999% purity) N<sub>2</sub> and He, oil-free valves and gas regulators were used for the free space correction and measurement. Relative pressure (P/P<sub>0</sub>) range for BET analysis was taken from 5.10<sup>-5</sup> to 0.3. Pore sizes were determined using DFT N<sub>2</sub> model for the cylindrical pores geometry, with relative pressure (P/P<sub>0</sub>) range from 0.003 to 0.1.

Infrared spectra were obtained on a PerkinElmer Spectrum 400 FTIR/FT-FIR Spectrometer equipped with a Pike Technologies GladiATR accessory with a germanium crystal. Diffuse reflectance UV-Vis spectra were collected on a Varian Cary 5000 UV-Vis-NIR spectrometer equipped with a Praying Mantis diffuse reflectance accessory and an environmental chamber (Harrick Scientific Products) and were referenced to BaSO<sub>4</sub>.

<sup>11</sup>B MAS NMR experiments were measured using a 16.4 T Magnex magnet and a home-built spectrometer (courtesy of Dr. David Ruben, FBML-MIT). All spectra were acquired using a 3.2 mm Varian magic-angle spinning triple-resonance probe, doubly tuned to <sup>11</sup>B and <sup>1</sup>H. Powdered samples were center-packed into 3.2 mm outer diameter (26 µl fill volume) ZrO<sub>2</sub> rotors with Torlon caps and Kel-F spacers. Spectra were acquired using a Bloch pulse sequence with short quantitative pulse widths (~15°, <sup>11</sup>B -  $\gamma_{B1}/2\pi = 53$  kHz) ideally suited to evenly excite three- and four-coordinated boron environments. High-power <sup>1</sup>H decoupling (<sup>1</sup>H -  $\gamma_{H1}/2\pi = 83$  kHz) was applied during signal acquisition. All experiments were acquired using a magic-angle spinning frequency,  $\omega_r/2\pi$ , between 15 and 17.5 kHz. Recycling time between each acquisition for each sample was between 2 and 5 seconds, with a total number of acquisitions ranged between 5,120 and 41,472 depending on the signal-to-noise. The magic-angle was adjusted by measuring the <sup>79</sup>Br rotational echoes of potassium bromide (KBr). <sup>11</sup>B spectra were referenced using a 0.1 M boric acid solution (H<sub>3</sub>BO<sub>3</sub>, 19.6 ppm) as a secondary standard relative to BF<sub>3</sub>·EtO<sub>2</sub>.<sup>1</sup>

<sup>11</sup>B MAS NMR is an extremely valuable and sensitive tool in determining local atomic-resolution information of boron-containing chemical systems. Both qualitative and quantitative

---

<sup>1</sup> Harris RK, Becker ED, Cabral de Menezes SM, Goodfellow R, Granger P (2001) NMR nomenclature. Nuclear spin properties and conventions for chemical shifts - (IUPAC recommendations 2001). *Pure & Appl Chem* 73:1795-1818.

information can be determined using  $^{11}\text{B}$  chemical shift ( $\delta_{\text{iso}}$ ), including pseudo-tetrahedral four-coordinated ( $^{14}\text{B}$ , -5 to 10 ppm) and trigonal planar three-coordinated ( $^{13}\text{B}$ , 10 to 45 ppm) environments. High field NMR (>11.7 T) provides an increase in spectral resolution largely due to the reduction of the second order quadrupolar broadening of the central transition under such condition, allowing good separation between  $^{13}\text{B}$  and  $^{14}\text{B}$  frequencies. At even higher magnetic fields (>14 T) multiple  $^{13}\text{B}$  environments can be further resolved. Figure S17 depicts two distinct  $^{13}\text{B}$  environments including borate<sup>2</sup>, boronic acids and esters<sup>3</sup>.

The resonance centered between 18 and 28 ppm is identified as the boron signal within the COF framework. The importance of studying these systems at high fields (16.4 T) is evident by the narrow linewidth (full-width at half maximum) obtained at  $\sim 6$  ppm (1.3 kHz) wide. The improvement is notable as previous studies at lower magnetic field (7 T) did not provide clear spectral resolution between  $^{14}\text{B}$  and  $^{13}\text{B}$ , nor between various  $^{13}\text{B}$  environments (i.e., boric acid and organic borates<sup>4</sup>). The spectral lineshape is Gaussian-like, which is indicative of a distribution of similar boron environments, this slightly disordered B environment could be caused by COF packing within the system.<sup>5</sup> This finding is consistent with the powder XRD data whereas a lower-degree of crystallinity was observed. Simulations of the  $^{11}\text{B}$  spectra show the quadrupolar coupling constant of the  $^{11}\text{B}$  in THT-COF is 2.8 (0.2) MHz with a high asymmetry parameter ( $\eta > 0.5$ ) consistent with the local  $C_{2v}$  symmetry about the boron site. Due to the distribution of sites within the  $^{13}\text{B}$  resonance it is difficult to ascertain an exact  $^{11}\text{B}$  isotropic shift, although an estimate of  $27 \pm 2$  ppm (center-of-gravity-shift is 23 ppm and left-edge-shift is 28 ppm) is consistent with crystalline model compounds of similar nature.<sup>3</sup> The concentration of B atoms to guest molecules is 6:1; if the guest was datively binding to a boron forcing a change in coordination one could expect up to  $\sim 15\%$   $^{14}\text{B}$ . The absence of a sharp boron resonance at lower frequency (10 to -5 ppm) indicates no  $^{14}\text{B}$  formation exists within the COF (i.e., < 0.5 % of total B environments).

---

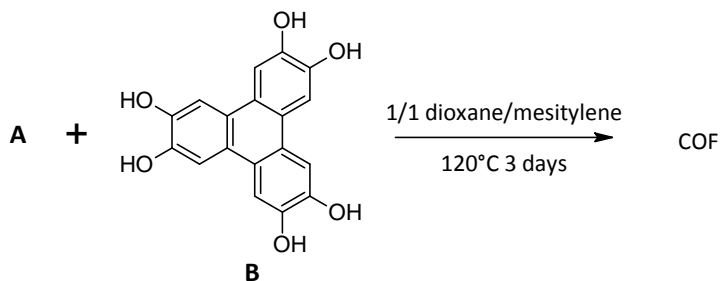
<sup>2</sup> Kroeker S, Stebbins JF (2001) Three-coordinated boron-11 chemical shifts in borates. *Inorg Chem* 40:6239-6246.

<sup>3</sup> Weiss, JWE, Bryce DL (2010) A Solid-State B-11 NMR and Computational Study of Boron Electric Field Gradient and Chemical Shift Tensors in Boronic Acids and Boronic Esters. *J Phys Chem A* 114:5119-5131.

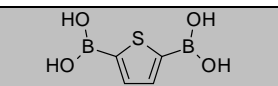
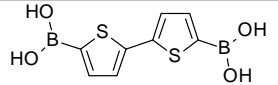
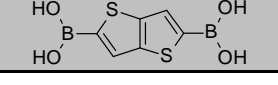
<sup>4</sup> Côté AP, Benin AI, Ockwig NW, O'Keeffe M, Matzger AJ, Yaghi OM (2005) Porous, crystalline, covalent organic frameworks. *Science* 310:1166-1170.

<sup>5</sup> Michaelis VK, Aguiar PM, Kroeker S (2007) Probing alkali coordination environments in alkali borate glasses by multinuclear magnetic resonance. *J Non-Cryst Solids* 353:2582-2590.

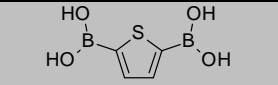
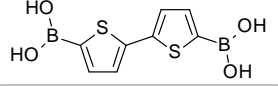
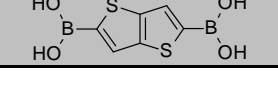
## B. Methodology for T-COF Synthesis.



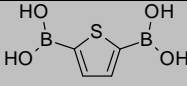
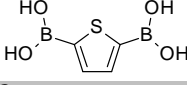
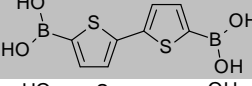
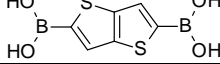
**Table 1.** Methodologies screenings. a) 8 days b) P = 150 W, 30 min

A	Sealed Tube	Dean stark	Sealed Tube + 1% water	Microwave <sup>b</sup>	N <sub>2</sub> Sealed Bomb	Air Sealed Bomb
	T-cof 1	T-cof 2	T-cof 1 + T-cof 2	T-cof 2	T-cof 2	NR
	T-cof 3 <sup>a</sup>	NR <sup>a</sup>	NR <sup>a</sup>	NR	T-cof 3 <sup>a</sup>	T-cof 3 <sup>a</sup>
	T-cof 4	T-cof 4	T-cof 4	T-cof 4	T-cof 4	T-cof 4

**Table 2.** Screenings of the A/B ratio. a) 8 days NR = No Reaction

A	A excess	A 3/1 B	A 3/2 B	B excess
	T-COF 1 + T-COF 2	T-COF 1 + T-COF 2	T-COF 1	NR
	T-COF 3 + A <sup>a</sup>	T-COF 3 <sup>a</sup>	T-COF 3 <sup>a</sup> + B	Starting materials + trace of T-cof 3 <sup>a</sup>
	T-COF 4 + A	T-COF 4	T-COF 4	NR

**Table 3:** Maximum yields for T-COF 1 to 4: a) Sealed tube 3 days. b) Dean-stark. c) Sealed tube, 8 days

A	Products	Yields
	T-cof 1 <sup>a</sup>	56 %
	T-cof 4 <sup>b</sup>	82 %
	TT cof <sup>c</sup>	67 %
	ThT cof <sup>b</sup>	91 %

C. Figures

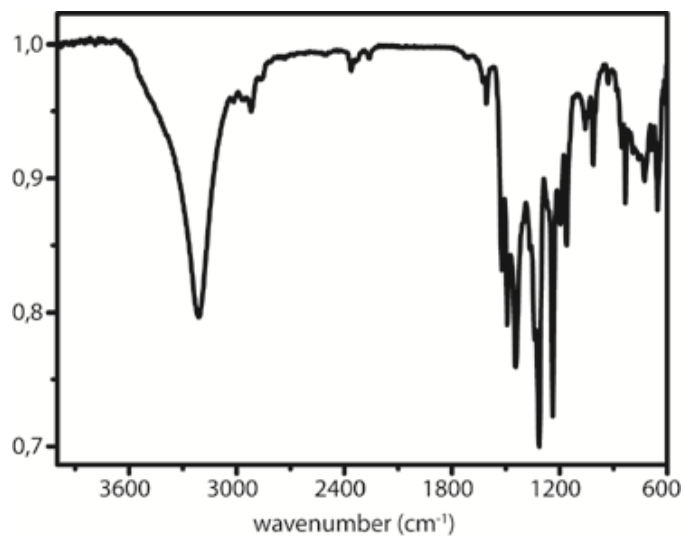


**Figure S1:** IR spectrum (Ge ATR) of T-COF 1.

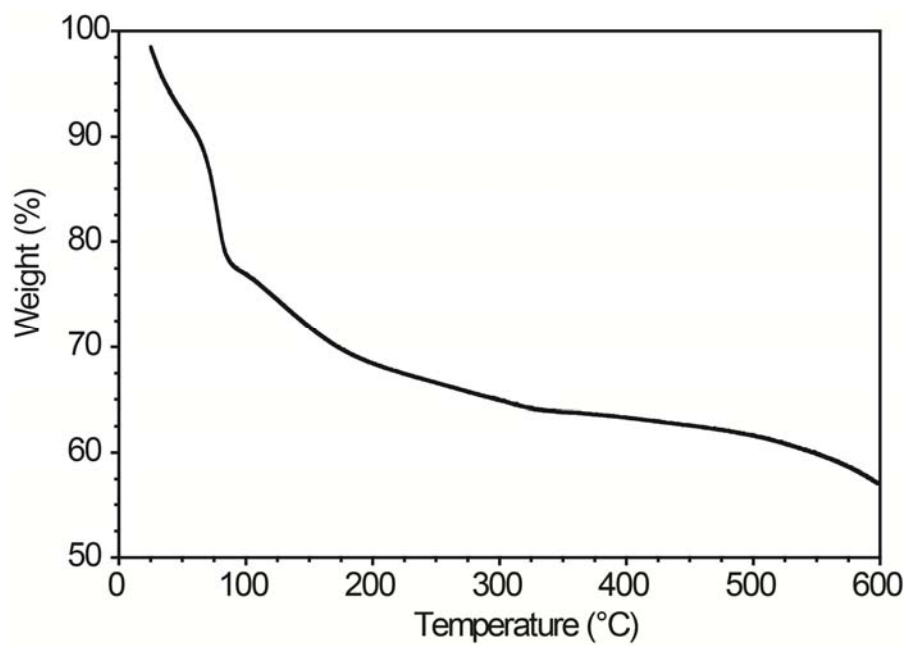


**Figure S2:** TGA of T-COF 1.

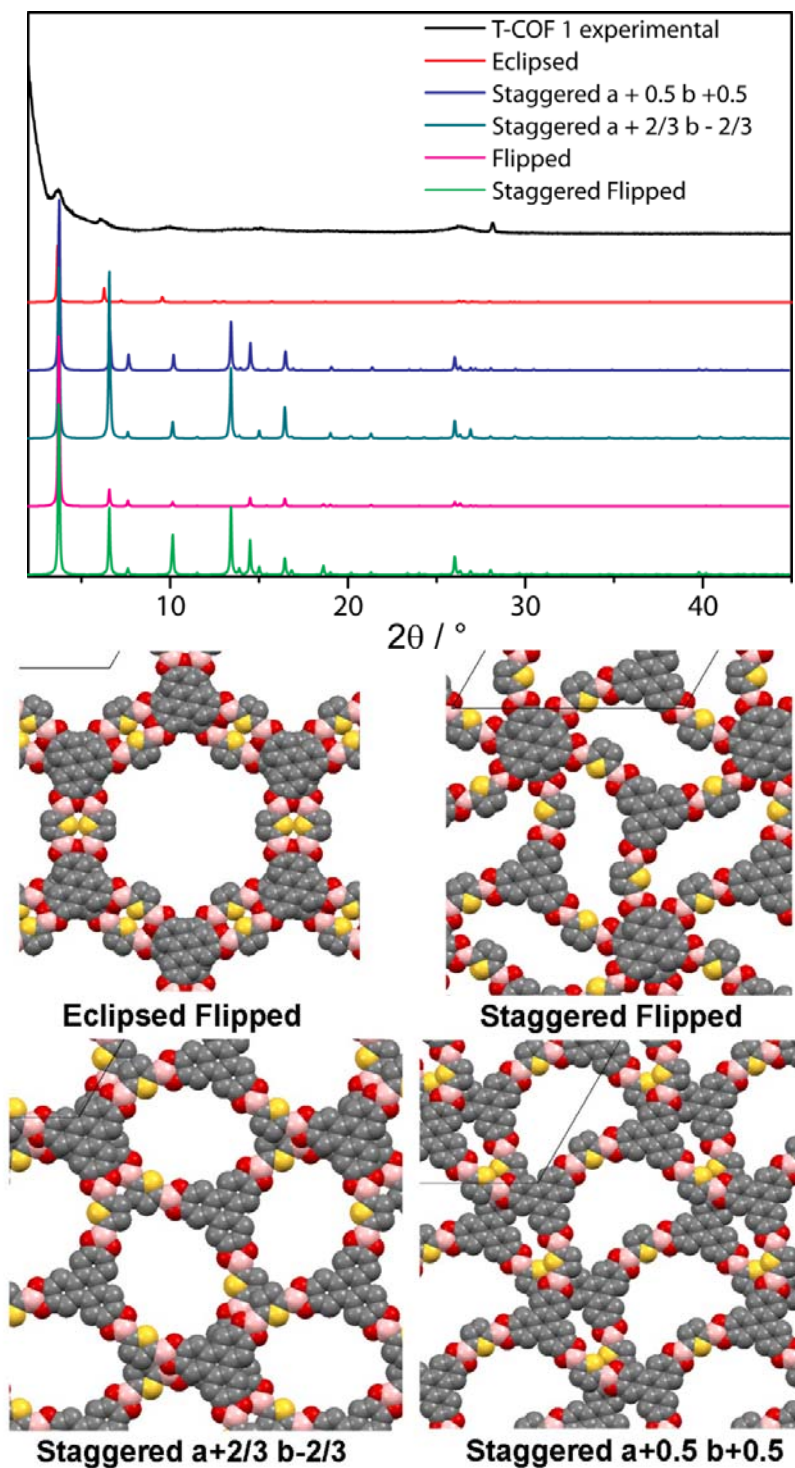


**Figure S3:** Experimental (black curve) and simulations of different possible structures of T-COF 1.

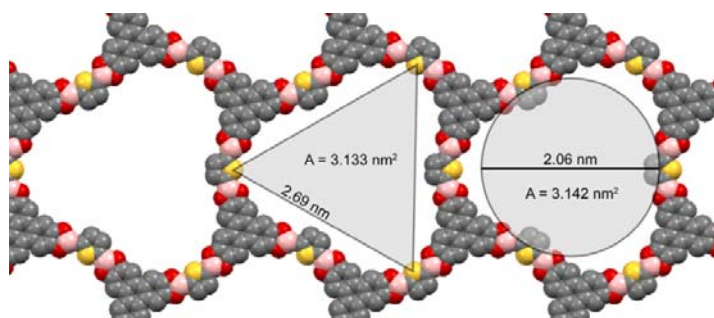
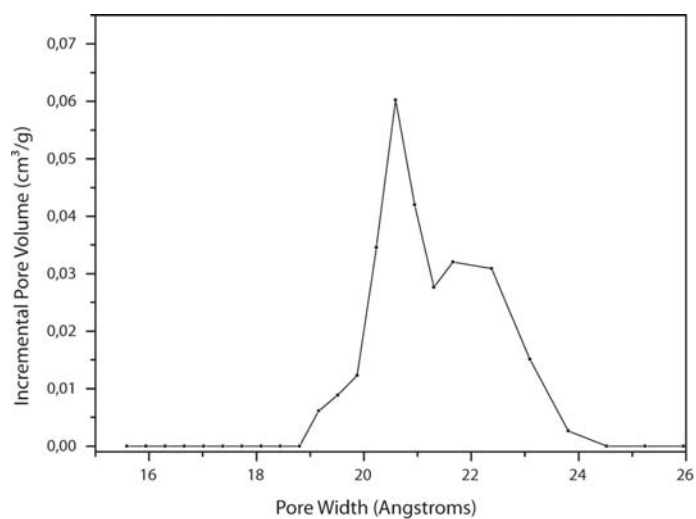


**Figure S4:** Top: DFT Pore size analysis of T-COF 1. Bottom: Simulated triangular cross-section and corresponding area (left) compared to the cylindrical cross-section given by DFT pore size analysis (right).



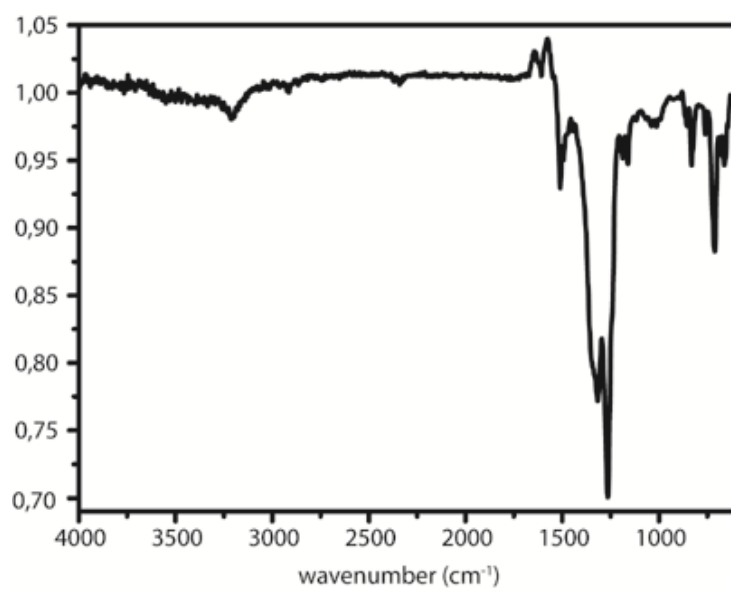


**Figure S5:** IR spectrum (Ge ATR) of T-COF 2.

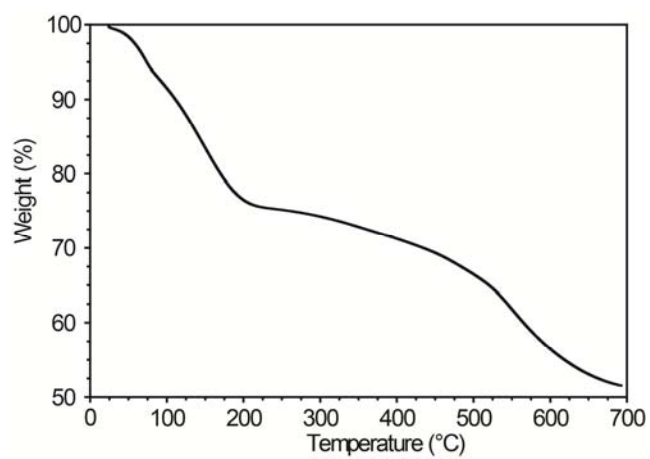


**Figure S6:** TGA of T-COF 2

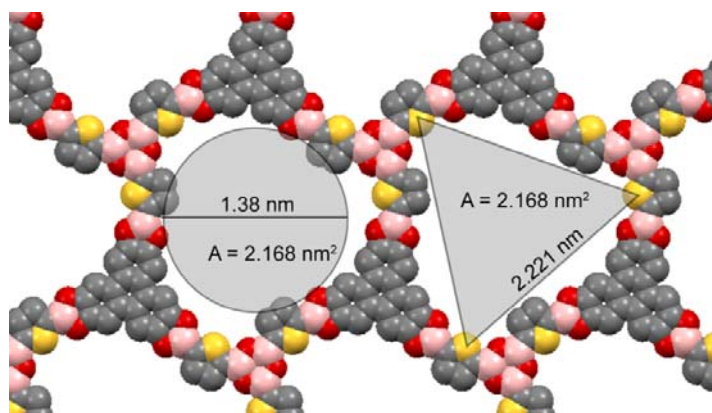
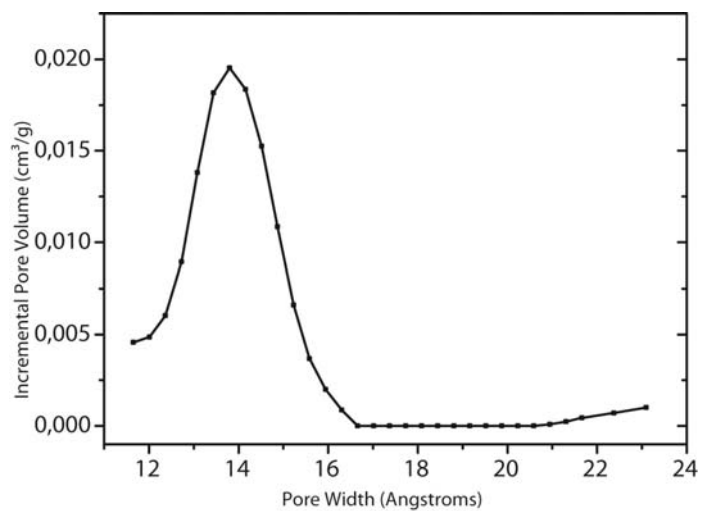


**Figure S7:** Top: DFT pore size analysis of T-COF 2. Bottom: Simulated triangle cross-section and corresponding area (right) compared to the cylindrical cross-section given by DFT pore size analysis.

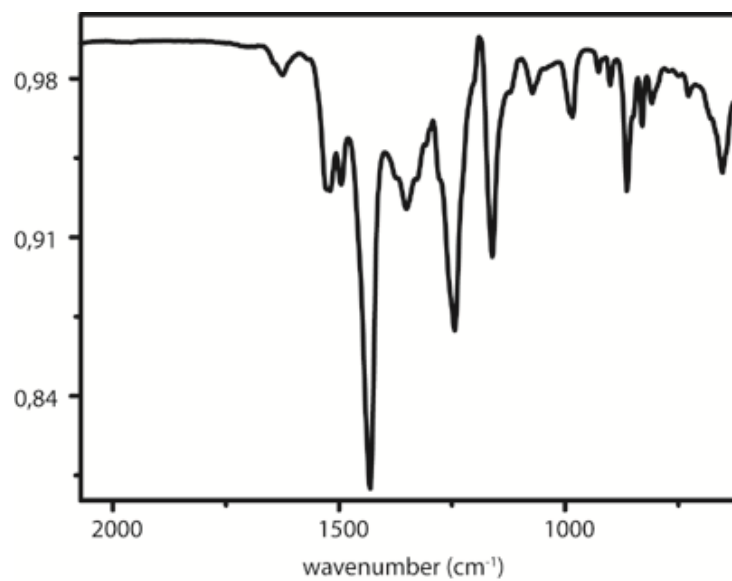


**Figure S8:** IR spectrum (Ge ATR) of T-COF 3.

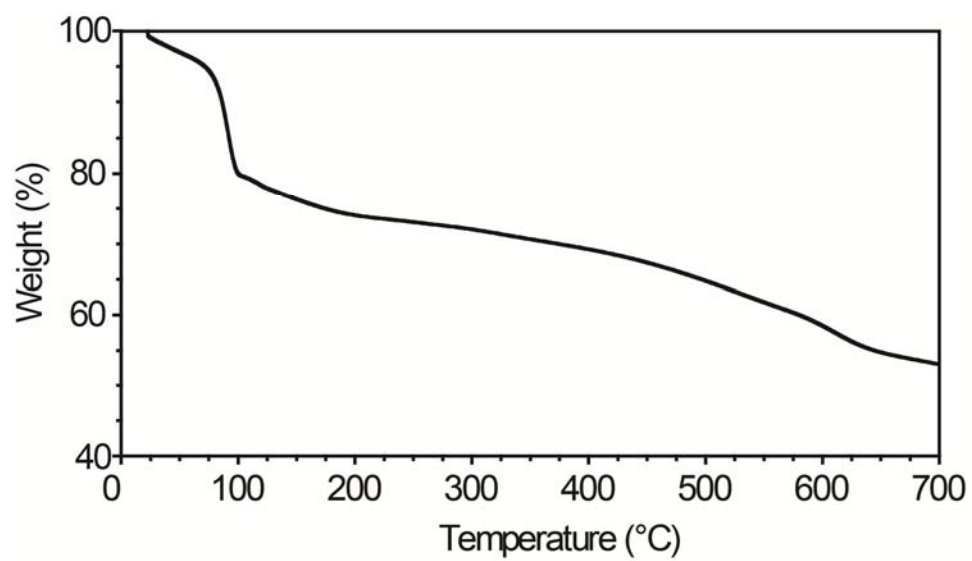


**Figure S9:** TGA of T-COF 3.

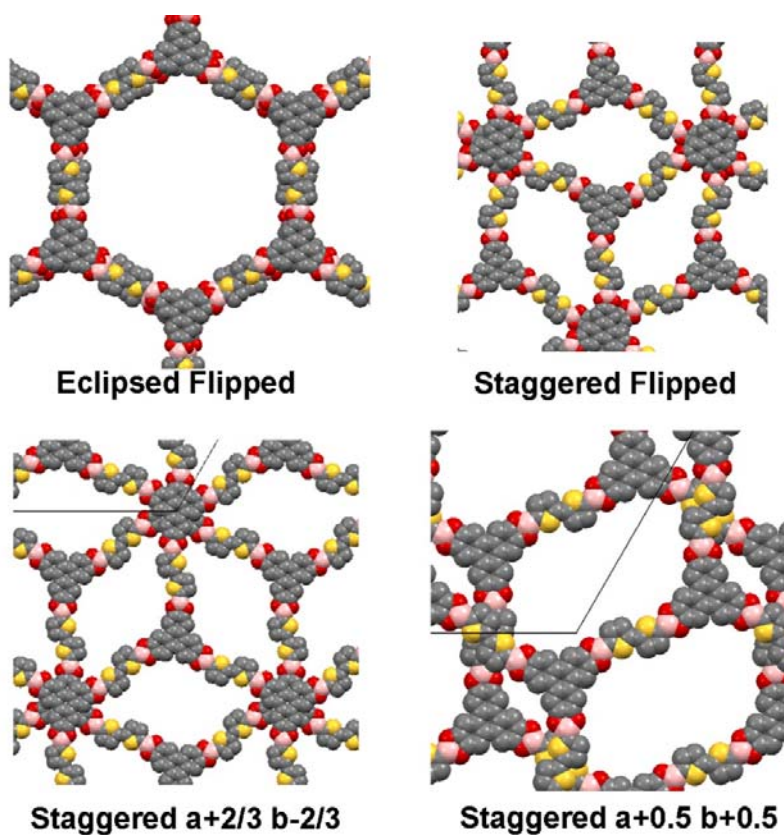
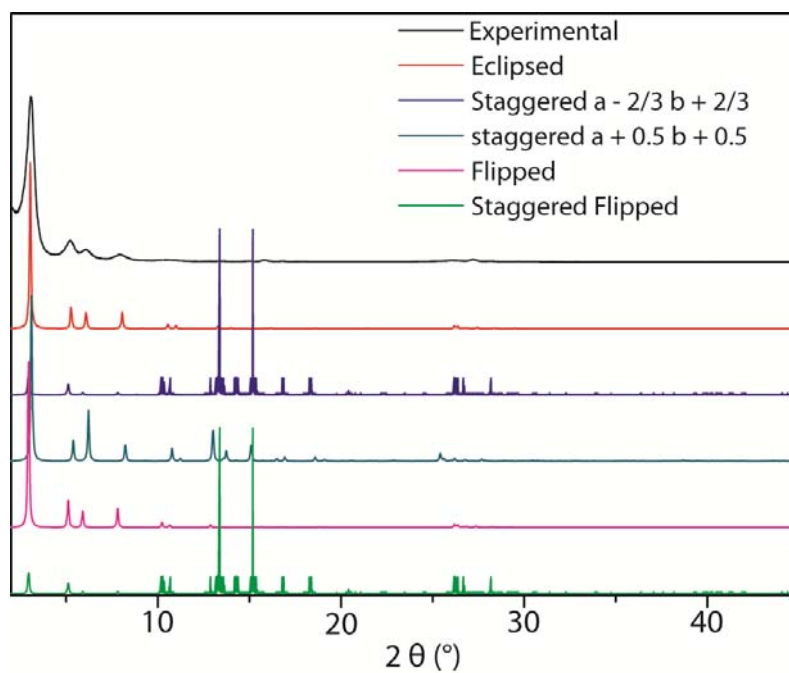


**Figure S10:** Experimental (black curve) and simulations of different possible structures of T-COF 3.

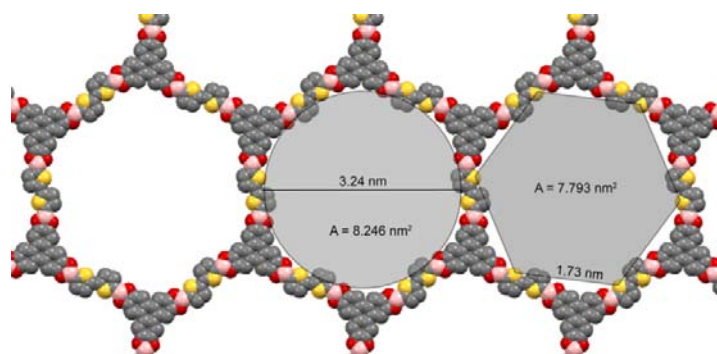
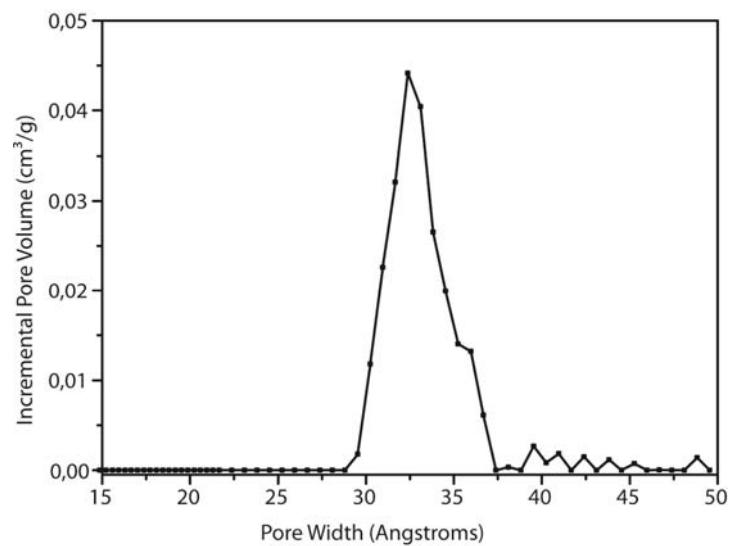


**Figure S11:** Top: DFT pore size analysis of T-COF 3. Bottom: Simulated hexagonal cross-section and corresponding area (right) compared to the cylindrical cross-section given by DFT pore size analysis (left).

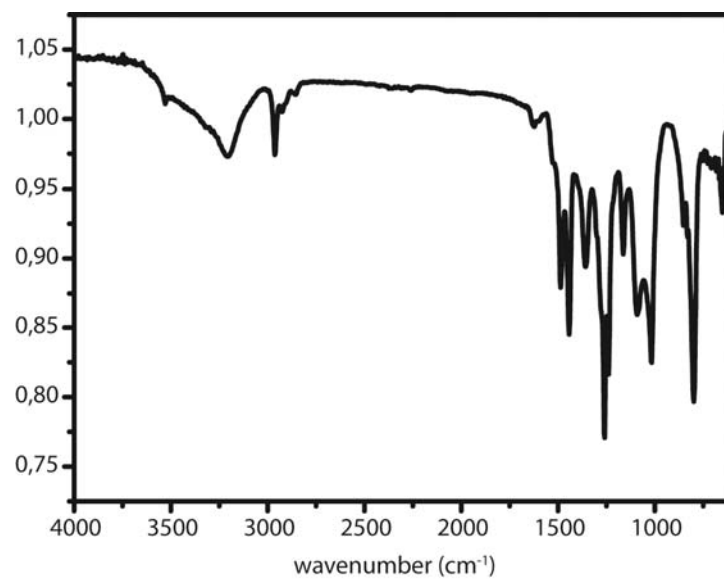


**Figure S12** IR spectrum (Ge ATR) of T-COF 4.

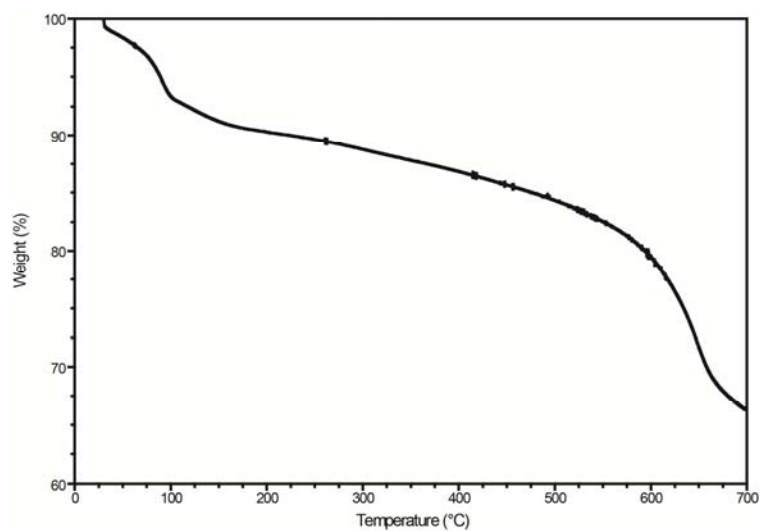


**Figure S13:** TGA of T-COF 4.

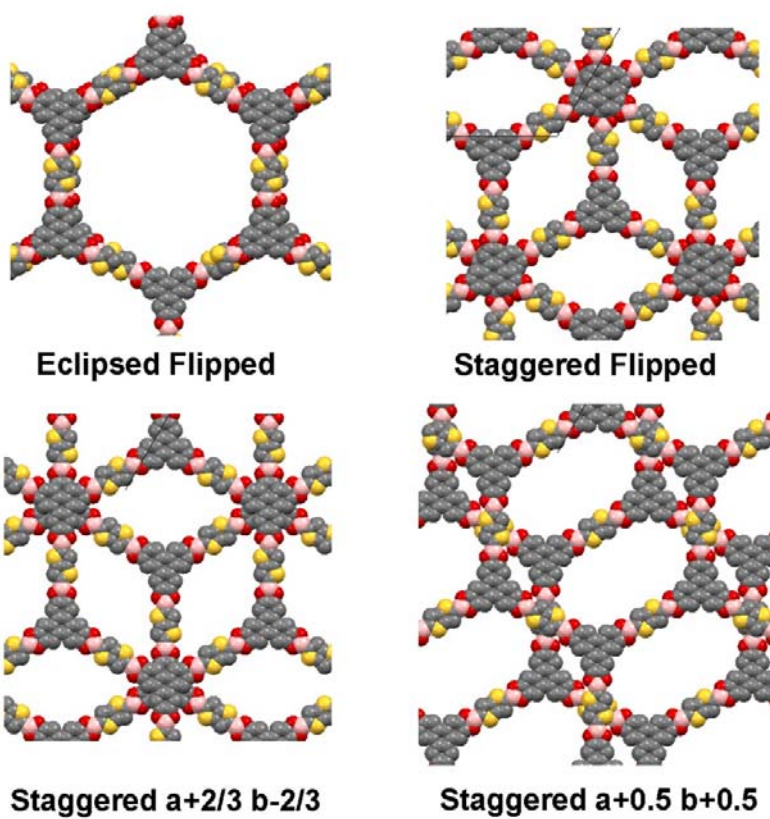
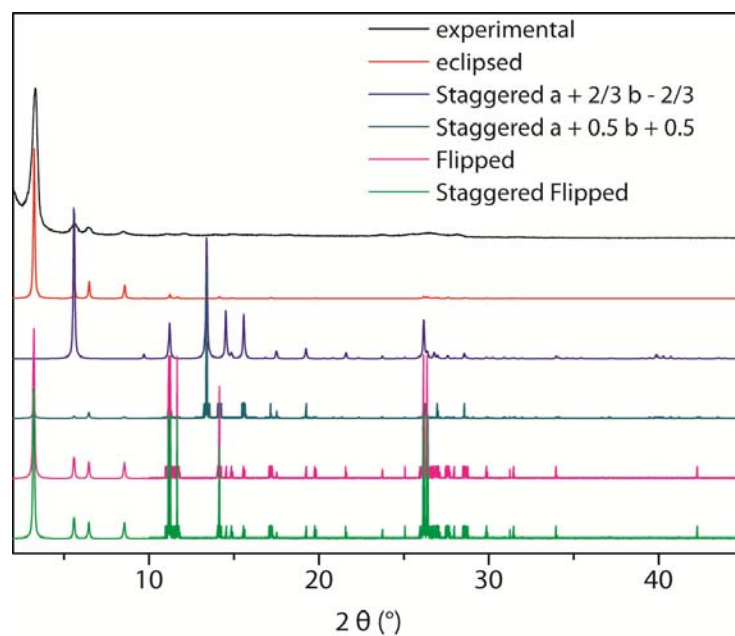


**Figure S14:** Experimental (black curve) and simulations of different possible structures of T-COF 4.

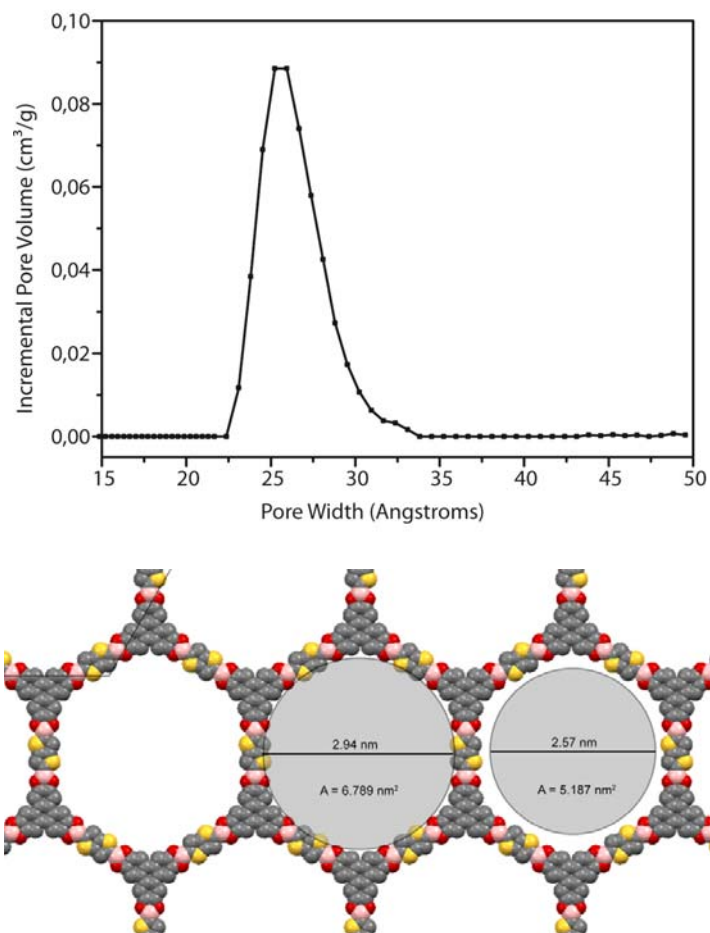


**Figure S15:** Top: DFT pore size analysis of T-COF 4. Bottom: Simulated disk cross-section (left) and corresponding area compared to disc cross-section given by DFT pore size analysis.



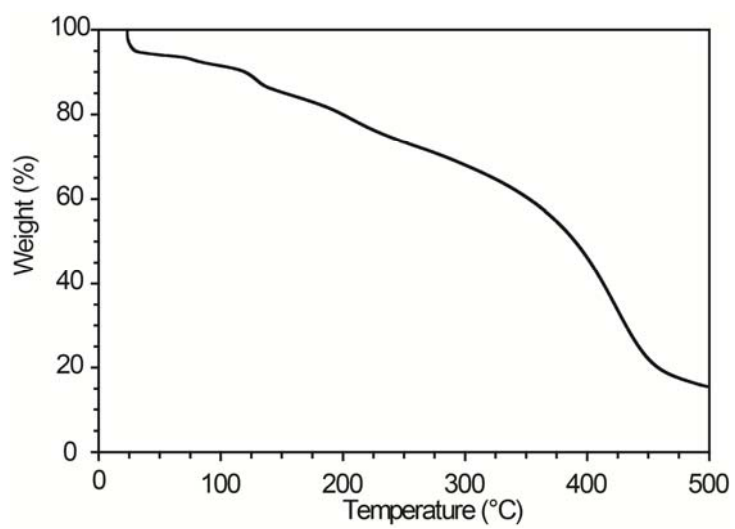


**Figure S16:** TGA of TCNQ-T-COF 4

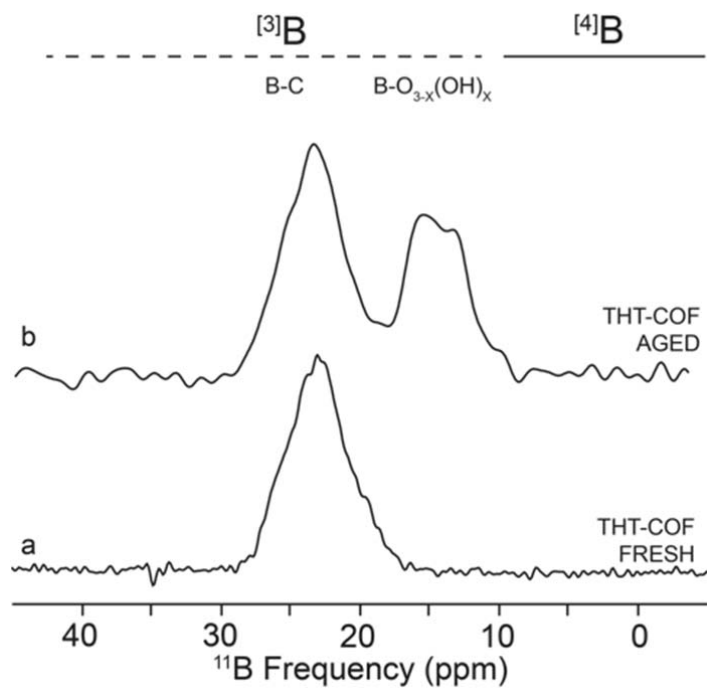


**Figure S17:**  $^{11}\text{B}$  MAS NMR ( $\nu_L = 223.4$  MHz) of T-COF 4 prepared fresh (a, 22 mg) and aged (b, 10 mg).

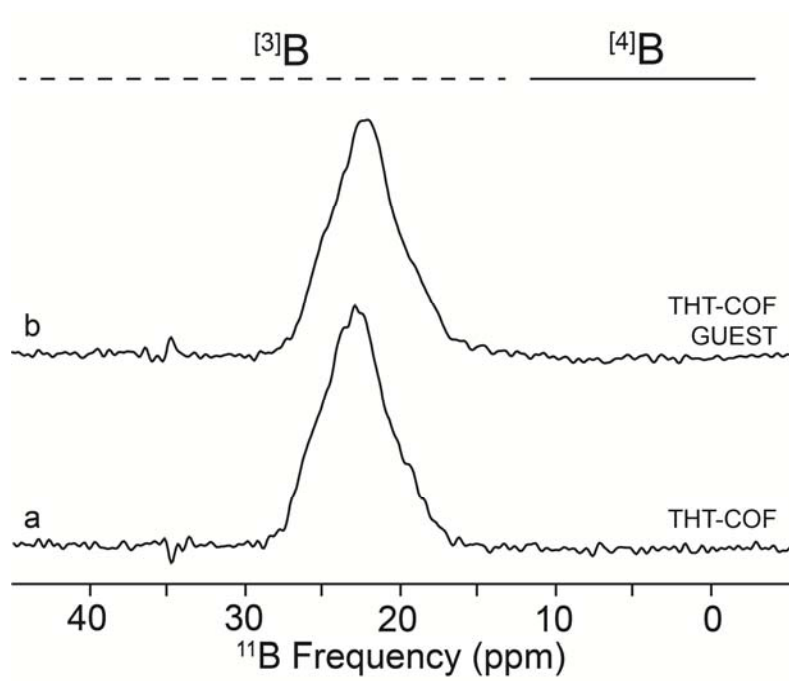


**Figure S18:**  $^{11}\text{B}$  MAS NMR ( $\nu_L = 223.4$  MHz) of freshly prepared T-COF 4 (a) and with the guest molecule TCNQ (b).